Open access • Journal Article • DOI:10.1007/BF00188507

Non-invasive measurements of granular flows by magnetic resonance imaging

Masami Nakagawa, S. A. Altobelli, Arvind Caprihan, Eiichi Fukushima ...+1 more authors

Institutions: Lovelace Respiratory Research Institute

Published on: 20 Jan 1993 - Experiments in Fluids (Springer Verlag)

Topics: Granular material, Flow velocity, Cylinder (engine) and Rigid body

DOE/PC/90184--T9

DE93 011448

NUCLEAR MAGNETIC RESONANCE STUDIES OF GRANULAR FLOWS

Technical Progress Report
to Pittsburgh Energy Technology Center
for the quarter ending 12/31/92

DE-AC22-90PC90184

We have hired Dr. L. Z. Wang as a postdoctoral fellow (not funded by this contract) who is interested in motion effects of flows. His Ph.D. is in physics and we anticipate that he will be a great help in this project. His term started early in December.

Task 2b (Material selection): We have identified all the suitable materials for the remaining experiments we plan to do. Further treatments to change material properties will be examined and will be reported as a part of the experimental results (Task 2e).

Task 2c (Imaging techniques): We have purchased and tested new rf preamplifiers that triple the signal-to-noise ratio. Thus, we are able to effect a 9-fold time saving of for an equal-quality image. We have obtained some fast images by the RARE technique that consists of a series of CPMG echoes with phase encoding before each echo and removal of the encoding after each echo. We have made a good quality, modest resolution, e.g., 1%, concentration image in approximately 100 ms. We still need to optimize our new shielded gradient coils (see last quarterly report) and we have not made fast velocity images but these imaging times are better than our previous times by two to three orders of magnitude.

Task 2e (Drum experiment): We have completed our first full manuscript on granular flow and sent it for review to the journal Experiments in Fluids. It is attached to this report. Further, we are in the process of understanding the relationship between the standard diffusion coefficient measurements in liquids by NMR and granular flows. In particular, we have examined the image attenuation as a function of "diffusion" sensitizing gradients associated with Stejskal-Tanner diffusion experiments. Our preliminary results are that the log of the echo amplitude decreases approximately linearly with the square of the gradient so that we can arrive at a diffusion coefficient image. We will continue along this line of attack and try to correlate the results with other data (such as the energy deposition images described in the last quarterly report) and with fluctuation parameters.

20 January 1993

Project Manager

Non-invasive Measurements of Granular Flows by Magnetic Resonance Imaging

M. Nakagawa[1], S. A. Altobelli[2], A. Caprihan[3],
E. Fukushima[4] and E.-K. Jeong[5]

DE-AC22-90PC90184

Lovelace Medical Foundation
2425 Ridgecrest Drive, SE
Albuquerque New Mexico 87108
USA

(1) Visiting Scientist
(2)(3)(4)Scientist
(5)Postdoctoral Fellow
at Lovelace Medical Foundation

Non-invasive Measurements of Granular Flows by Magnetic Resonance Imaging

DE-AC22-90PC90184

M. Nakagawa[1], S. A. Altobelli[2], A. Caprihan[3],
E. Fukushima[4] and E.-K. Jeong[5]

Lovelace Medical Foundation
2425 Ridgecrest Drive, SE
Albuquerque New Mexico 87108
USA

(1) Visiting Scientist
(2)(3)(4)Scientist
(5)Postdoctoral Fellow
at Lovelace Medical Foundation

ABSTRACT

Magnetic Resonance Imaging(MRI) was used to measure granular flow in a partially filled, steadily rotating, long, horizontal cylinder. This non-invasive technique can yield statistically averaged three-dimensional concentrations and velocity profiles anywhere in the flow of suitable granular materials. First, rigid body motion of a cylinder filled with granular material was studied to confirm the validity of this method. Then, the density variation of the flowing layer where particles collide and dilate, and the depth of the flowing layer and the flow velocity profile were obtained as a function of the cylinder rotation rate.

1. Introduction

Rotating cylinders are used in chemical and metallurgical industries for processes such as comminuting, mixing, ball milling, and drying granular and powder materials. There have been several experimental studies of transverse bed motion and radial segregation of granular materials in rotating cylinders. Although most of them are qualitative studies for design purposes, some experiments emphasize the dynamic behavior of flow.

Henein, et al. (1983) characterized different modes of granular bed motion by the "Bed Behavior Diagram" which is a plot of bed depth vs. rotational speed. Klein and White (1990) performed a rapid-flow experiment in a rotating cylinder in an airplane to show the effect of gravity on the dynamic angle of repose. Rajchenbach (1990) studied the transition from the discrete to the steady mode of flow in a rotating cylinder and also established a relationship between the surface current and the dynamic angle of repose. Segregation is expected whenever a flow consists of more than one component each having different particle properties such as density, size, and shape. Nityanand, et al. (1986) investigated radial segregation due to size differences of spherical solids for different modes of granular bed motion.

The above studies of dynamic behavior of granular flows in a rotating cylinder have been done by the observation of flow through a transparent section of the cylinder. Thus, these are non-contact measurements but mostly with end effects and without information from inside the flow. Other techniques to measure properties of multi-phase flows, especially particulate multi-phase flows, employ focused light, sound waves, or ion beams. Unfortunately, most of them suffer signal attenuation due to opacity or scattering at dense concentrations. Tracer methods can yield flow information deeper in a sample, but obtaining concentration information is difficult, if not impossible. Acquisition of an ensemble average of flow properties is time consuming, and there is little chance of these methods leading to the detailed analysis of velocity and fluctuational parameters. On the other hand, x-ray methods like CAT scans may be used to obtain concentration

data but not velocity. Thus, the lack of good techniques to study granular flows has been a most pressing concern for theoreticians and design engineers.

Magnetic Resonance Imaging (MRI), a subfield of nuclear magnetic resonance (NMR), is a non-invasive technique which works well deep in the sample, does not require any mechanical markers, and has no preferred orientation of measurement. The technique has recently been used to study the migration of particles in a concentrated suspension being sheared in a Couette geometry (Graham, et al., 1991; Abbott, et al., 1991). The velocity and concentration behavior of concentrated suspensions in a circular pipe using MRI has also been studied (Majors, et al., 1989; Altobelli, et al., 1991). Particles (polymethyl methacrylate and divinyl-benzene styrene copolymer) used in those experiments gave no NMR signals themselves, but the mixture concentrations and, for the case of the circular pipe, the longitudinal velocity profiles of the liquid phase were successfully obtained for solid phase concentration up to 39%.

The application of MRI to solid materials is still in its infancy and, to our knowledge, no flow studies of solids have been performed. For all practical purposes, the easiest nuclei to image by MRI are protons in the liquid state. Therefore, we avoid the solid state NMR problem by using solid particles containing protons in the liquid state so that, in effect, we study flows of solids by liquid state MRI.

2. MRI Background

An atomic nucleus with a magnetic moment precesses around the magnetic field like a spinning top precesses about the direction of gravity. There is a unique precession frequency called the Larmor frequency for each atomic nucleus in a particular strength of magnetic field. A known spatial variation of the magnetic field will cause the nucleus at each point to execute a different Larmor frequency. MRI measures the distribution of signals as a function of this frequency and relates it to the spatial distribution of nuclear spins. This technique is now widely used for non-invasive diagnosis in clinical medicine.

The use of NMR for studying flowing samples is more complex than it is for measuring static samples but it offers a unique technique for non-invasively studying the detailed concentration and flow behavior anywhere in the flow regardless of optical or acoustic opacity. Basics of MRI for studying flowing fluids have been described elsewhere (Caprihan and Fukushima, 1990). Therefore, only a summary is given here.

A good way to visualize flows by MRI is to use non-invasive tags. We selectively irradiate the atomic nuclei in a grid pattern prior to making an image so that no signals are induced from the pattern in a subsequent image. [For example, see Mosher and Smith, 1990, and references therein.] The grid pattern evolves, during the delay between the tagging and the imaging, according to the flow pattern.

For the quantitative evaluation of velocities, we use the so-called phase method in this work. It works on the principle that the phase of the macroscopic magnetization comprised of the aggregate nuclear moments in an element of volume evolves in a manner depending on its motion in the presence of a magnetic field-gradient. We obtain the velocity information from the measured phase behavior of the magnetization in each image voxel. By applying the magnetic field gradient in a certain sequence, we make the phase shift proportional to the average velocity in the voxel with the proportionality factor an experimentally controllable parameter called the first moment of the gradient.

In the actual experiment, we add an embellishment to the procedure to eliminate phase shifts of the signal caused by factors other than the velocity of moving spins. These factors include electronic delays in the amplifier circuits, missetting the time origin during data acquisition, etc. If we write the incremental phase shift $\Delta\phi$ as

$$\Delta\phi = \gamma\, m_1\, V + \textit{other phase shifts} \qquad (1)$$

where γ is the gyromagnetic ratio, which is identical for all protons, and m_1 is the first moment, we can eliminate the effect of other phase shifts by repeating the experiment for various values of m_1 and obtaining the velocity V from a linear fit of $\Delta\phi$ vs. $\gamma\, m_1$ for each voxel (Caprihan, et al., 1990).

3. Experimental

Protons are best suited for MRI because of their strong signal as well as of their abundance in nature. In this study we used mustard seeds which yield excellent proton NMR signals from their oils. Based on measurements of a few hundred representative seeds, their average diameter is 1.7 ± 0.2 mm, the average density is 1.3 g/cm^3, and the average coefficient of restitution is 0.56 when they are dry and at room temperature. The coefficient of restitution was obtained by performing "single bounce" experiments against a hard flat surface.

We used a NMR imager/spectrometer (Nalorac Cryogenics Corp) with a 1.9 Tesla superconducting magnet (Oxford) having a bore diameter of 31 cm. After the insertion of gradient/shim coils and the rf probe, the useful bore is 12 cm and the volume that can be imaged is approximately a sphere of diameter 8 cm. Figure 1 shows a schematic view of the experimental set-up with the long nonmagnetic shaft which is required to keep the motor far from the magnet. We use a dc servo motor (12FG) and a controller (VXA-48-8-8) made by PMI.

We used two acrylic cylinders to rotate the seeds. First, a 585 mm long cylinder with an inner diameter of 88 mm was half-filled with mustard seeds. Later, a smaller cylinder of length 300 mm with an inner diameter of 70 mm was half-filled with mustard seeds and inserted into the larger cylinder. The gap between the concentric cylinders was filled completely with mustard seeds

which formed a ring of uniform concentration undergoing a rigid body rotation with a predictable concentration and velocity profiles which were then used as references at each rotation speed.

Our MRI experiment for granular flow selects a 8 mm thick slice, near the center of the cylinder and transverse to the cylinder axis (z-direction), with an inplane resolution of 0.8mm. The orthogonal components of the velocity, V_x and V_y, were measured in two independent experiments with a total measurement time of approximately 15 minutes. MRI measures average flow properties over this duration and within each voxel through the slice. The images are smoothed to enhance the signal-to-noise ratio, and this causes some rounding of velocity and concentration profiles at the boundaries including the free surface.

4. Results

4.1 Rigid Body Rotations

Figures 2(a) and 2(b) are the concentration profiles of fully packed mustard seeds along a typical diameter in the 88mm diameter cylinder undergoing rigid body rotation at 30 rpm and 53 rpm, respectively. Such uniform radial profiles assure that the method yields accurate concentration profiles for these rotating samples. The discreteness of these profiles is caused by the thickness of the slice which is only about five particle diameters.

Figures 3(a) and 3(b) show the x and y velocity profiles of the same sample at the same rotation rate of 30 rpm and 53 rpm. Both velocity components vary linearly as $\Omega \cdot x$ or $\Omega \cdot y$, as predicted, where Ω is the rotation rate and x and y are displacements. The ratio of maximum V_x (or V_y) for the flow with 30 rpm to that with 53 rpm is 0.56 which is close to the predicted value. This ratio between two different velocity components at different rotation speeds also persists everywhere in the flow, demonstrating the accuracy of these velocity measurements.

4.2 Concentration and Bed Motion in A Rotating Cylinder

Bed motions in a partially filled rotating cylinder can be characterized in different modes; slipping, slumping, rolling, cascading, cataracting, and centrifuging (Henein, et al.,1983). These motions are influenced by rotation speed, bed depth, cylinder diameter, and particle properties. NMR concentration images of seeds at 30 and 50 rpm (Fig. 4) show flows in the rolling and the cascading modes, respectively. These modes are characterized by the shapes of free surfaces; flows in the rolling mode by its flat surface and the cascading mode by its s-shape. Colors are assigned to concentrations as indicated by the color bar; light-to-dark blue for less concentrated regions and white-to-yellow for more concentrated regions. The thickness of the flowing, dilated layer, colored light blue, increases with the rotation speed and this will be discussed later. The rings surrounding the inner cylinder contains solidly packed mustard seeds for velocity and

concentration reference, as described earlier, and their colors are uniform for each image as expected.

Figure 5 shows concentration plots for these flows along a cut through the center of the cylinder and perpendicular to the free surface. The reduced concentration close to the free surface caused by particle collisions is clearly visible. We have also noticed that there is always a slight concentration gradient even in the nonflowing portion with the maximum next to the cylinder wall, and this is undoubtedly caused by dynamic packing effects.

4.3 Tagging Experiments

Figure 6 shows the results of a tagging experiment in which a rectilinear grid pattern is imprinted in the seeds and imaged after various delays to display the evolution of the pattern caused by the flow at a rotation speed of 18 revolutions per minute. There are delays of 1, 10, 20, 50, and 100 ms between tagging and imaging. It is easy to see the rigid-body rotation of the seeds near the cylinder wall as well as the flow that takes place across the free surface. Velocity and shear may be calculated from the evolution of particular cells as a function of delay time.

4.4 Velocity Profiles of Seeds

Velocity information can be presented in many ways including vector or polar form. For vectoral representation of velocity, its components may be decomposed into x and y directions, in the directions parallel and perpendicular to the flow, or any other desired directions. For polar representation, velocity information is separated into its magnitude and angle.

Figure 7 shows components of velocity parallel and perpendicular to flows at 30, 53, and 78 rpm obtained by the phase method with phase maps for each velocity image. The color bar indicates the velocity components from maximum in the direction of the flow at the top of the color bar to maximum in the opposite direction at the bottom of the color bar. The color assignment for velocity component perpendicular to the flow is exactly the same, except its orientation is rotated counterclockwise by 90 degrees. These images show one of the pitfalls of the phase method and the usefulness of the reference ring. The two locations of the background color (brownish-yellow), i.e., zero velocity, should be 180 degrees apart on the ring, and rotated 90 degrees between the two orthogonal components. In these images, the orthogonality is quite good but the absolute phase reference, i.e., the cancellation of the last term in Eq. (1), is not perfect, especially in the perpendicular component at 30 rpm. With the reference ring, this error is correctable.

Figure 8 shows a typical profile of velocity along the free surface for flow at 30 rpm. It was obtained three bead diameters deep in the flow and indicates that the velocity is not symmetric around the center, i.e., flow accelerates in the flowing direction even after it passes the center. Our preliminary results show that the surface mass-flux, calculated from these velocity data together

with concentration data, is asymmetric as well, with the sense of asymmetry depending on the rotation speed; the peak in the mass-flux moves from the upper half to the lower half as the rotation rate is increased.

Figure 9 shows a velocity profile of mustard seeds in the rolling mode at 17 rpm along a line AB (B at the bottom of cylinder) going through the center of the 88mm diameter cylinder and perpendicular to the free surface. We identify three different regions. The region where the seeds are in rigid body rotation is indicated r-r'. The flowing layer goes from f to r' and consists of a constant shear part f-f' near the free surface and a deeper, variable shear region f'-r'. A meaningful zero-velocity point is r' where seeds above this point flow with respect to those in rigid body rotation.

Figure 10 shows that the thickness F of a flowing layer, defined as r'-f on Fig. 9, increases monotonically with rotation rate but at an ever decreasing rate, reflecting the fact that the average mass flux is not proportional to the rotation rate, especially at the slower speeds. Even at the slowest flow measured, 2.4 rpm, there was a significant number of seeds in the flowing layer.

Figure 11 shows polar representations of velocity (speed and angle images) for flows at 30, 53, and 78 rpm. Speeds are obtained as square roots of sums of squares of x and y velocity components. This time, the color gradation ranges from zero (black) to maximum (white). These speed images, together with the concentration images, are perhaps the easiest of the images to understand. The speed is plotted without regard to the direction of motion. The flowing region is clearly shown by the lighter color near the free surface whereas the solid body rotation region shows the expected concentric color scheme. The reference ring is uniform in color and it becomes lighter as the rotation rate increases.

The speed images are complemented by angle images. The angle of averaged velocity vector in each voxel is calculated as arctan (V_y/V_x) and increases in the counterclockwise direction from the 9 o'clock position. The point where all the colors come together is the stagnation point where the velocity is zero in the laboratory frame. This is close to but not the same as the point r' of Fig. 9 because r' was defined by the onset of flow with respect to the seeds undergoing solid body rotation. Furthermore, the stagnation point may not even lie on line AB of Fig.9. The laboratory frame velocity at r' is the product of the angular velocity Ω and the radial distance s from center of the cylinder. The seed just above r' barely flows but moves in the same direction in the laboratory frame as the seed immediately below it; i.e., in the opposite direction as the faster main flow near the free surface. In contrast, the seeds above the stagnation point move in the direction of main flow. Thus, the stagnation point is where the flowing velocity with respect to the seeds in solid body rotation cancels the effect of solid body rotation at that point. The stagnation point moved deeper and also upstream as the rotation speed increased.

5. Summary

MRI was used to non-invasively measure concentration and velocity profiles of flowing mustard seeds in a half-filled steadily rotating cylinder. Concentrations and any component of velocity can be obtained anywhere in the sample. From these data we can derive profiles and distributions of shear, mass flux, acceleration, etc. and such results will be described in subsequent papers. To the authors' knowledge this is the first such non-invasive measurements of what is happening inside gas-solid flows. Making these measurements deep in the sample has proven to be straightforward and the global data acquisition can be done in a relatively short time.

Acknowledgments

This work was sponsored, in part, by the U.S. Department of Energy, Pittsburgh Energy Technology Center via Contract #DE-AC22-90PC90184 and the U.S. Department of Energy, Office of Basic Energy Sciences via Contract #DE-FG04-90ER14087. Additional financial support was provided by the sponsors of the Petroleum Research Fund which is administered by the American Chemical Society . The idea that the horizontal, rotating cylinder flow of granular material is well suited to NMR was that of R.C. Givler of Sandia National Laboratories. We also acknowledge the help of Heyning Cheng, a summer undergraduate research assistant.

References

Abbott, J.R., Tetlow, N., Graham, A.L., Altobelli, S.A., Fukushima, E., Mondy, L.A., and Stephens, T.S. 1991:Experimental observations of particle migration in concentrated suspensions: Couette flow. Journal of Rheology 35 (5), 773-795.

Altobelli, S.A., Givler, R.C., and Fukushima, E. 1991:Velocity and concentration measurements of suspensions by nuclear magnetic resonance imaging. Journal of Rheology 35 (5), 721-734.

Caprihan, A., Altobelli, S. A., and Benitez-Read, E. 1990: Flow-Velocity Imaging from Linear Regression of Phase Images with Techniques for Reducing Eddy Current Effects. J. Magn. Reson. 90, 71-89.

Caprihan, A and Fukushima, E. 1990: Flow Measurements by NMR. Physics Reports 198, 195-235.

Graham, A.L., Altobelli, S.A., Fukushima, E., Mondy, L.A., and Stephens, T.S. 1991: NMR imaging of shear-induced diffusion and structure in concentrated suspensions undergoing Couette flow. Journal of Rheology 35(1), 191-201.

Henein, H., Brimacombe, J.K., and Watkinson, A.P. 1983:Experimental Study of Transverse Bed Motion in Rotary Kilns. Metallurgical Transactions B 14B, 191-205.

Klein, S.P. and White, B.R. 1990 : Dynamic Shear of Granular Material Under Variable Gravity Conditions. AIAA Journal 28, No.10, 1701-1702.

Mosher, T.J. and Smith, M.B. 1990 : A DANTE Tagging Sequence for the Evaluation of Translational Sample Motion. Magn. Reson. Med. 15, 334-339.

Nitynnand, N., Manley, B., and Henein, H. 1986 : An Analysis of Radial Segregation for Different Sized Spherical Solids in Rotary Cylinders. Metallurgical Transactions B 17B, 247-257.

Rajchenbach,J. : Flow in Powders: From Discrete Avalanches to Continuous Regime. Physical Review Letters 65, Number 18, 2221-2224.

Figure Captions

Figure 1. Schematic view of the experimental apparatus with a magnetic resonance imager, a 1.9 T superconducting magnet, and a motor located about 3m away from the magnet.

Figure 2. Concentration profiles of fully packed seeds along an arbitrary diameter. (a) at 30 rpm, (b) at 53 rpm.

Figure 3. (a) Profiles of x-component of velocity of fully packed seeds, V_x, at 30 rpm and at 53 rpm along x=0.
(b) Profiles of y-component of velocity of fully packed seeds, V_y, at 30 rpm and at 53 rpm along y=0.

Figure 4. Concentration images of mustard seeds flowing in a half-filled cylinder at rotation speeds of 0, 30, and 53 rpm. The reference ring contains solidly packed seeds which do not flow. The white end of the color bar corresponds to the highest concentration.

Figure 5. Concentration profiles of flows at 0, 30, and 53 rpm. These profiles are along a line going through the center of the cylinder and perpendicular to the free surface. The free surface is at center and the filled half-cylinder is to the right. The two narrow "peaks" at the ends are caused by the reference ring.

Figure 6. Evolution of rectilinear grid pattern during the delays indicated from tagging to imaging. The mustard seeds are flowing in a half-filled cylinder rotating at 18 rpm.

Figure 7. Images of velocity components parallel and perpendicular to the free surface for seeds flowing at 30, 53, and 78 rpm in a half-filled cylinder.

Figure 8. Profile of velocity component along the free surface, actually three bead diameters deep in the flow, at 30 rpm. The flow goes to the right.

Figure 9. Schematic view of a motion of beads with the corresponding profile of flow velocity parallel to the free surface along a diameter perpendicular to the free surface in the rolling mode at 17 rpm. f is at the free surface and r at the cylinder wall. F is the sliding layer consisting of a constant shear portion f-f' and a variable shear portion r'-f'. The seeds from r' to r do not flow but rotate as a solid body so the velocity is $\Omega \cdot s$ where Ω is the rotation angular velocity and s is the distance from the center of cylinder.

Figure 10. Dimensionless thickness of the sliding layer F versus rotation speed.

Figure 11. Speed and angle images of flows at 30, 53, and 78 rpm. The color of the ring is uniform and changes as a function of angular velocity Ω for the speed images. On the other hand, the colors in the ring are independent of Ω for angle images. For the seeds undergoing rigid body rotation, i.e., those that are not close to the free surface, the colors are independent of not only Ω but also of the distances from the center of cylinder.

FIGURE 1

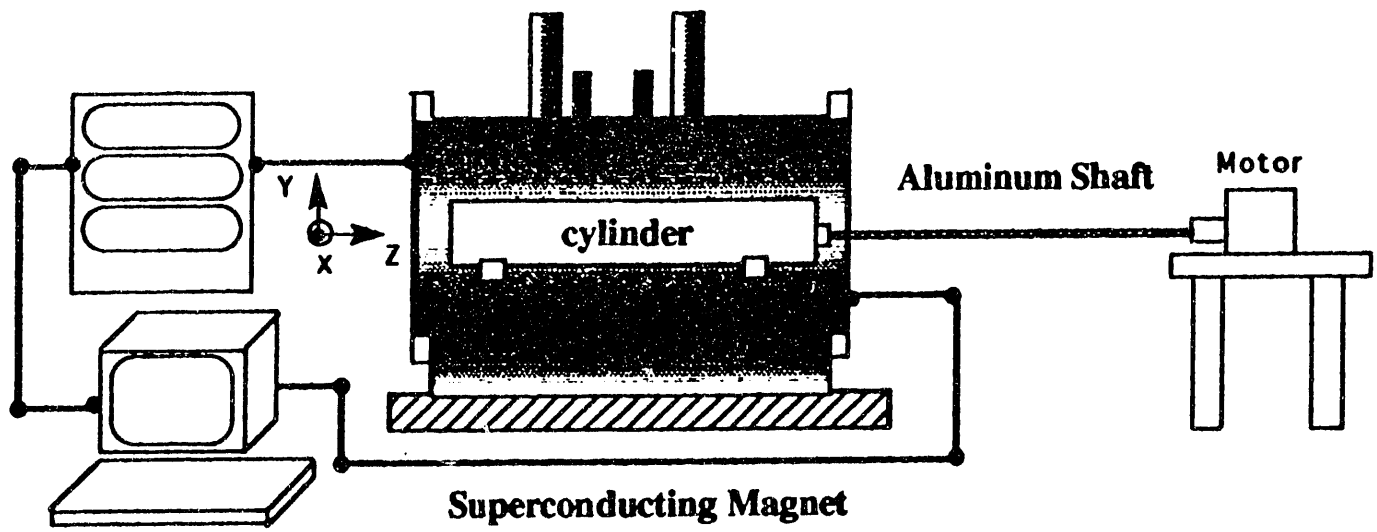

Magnetic Resonance Imager

FIGURE 2

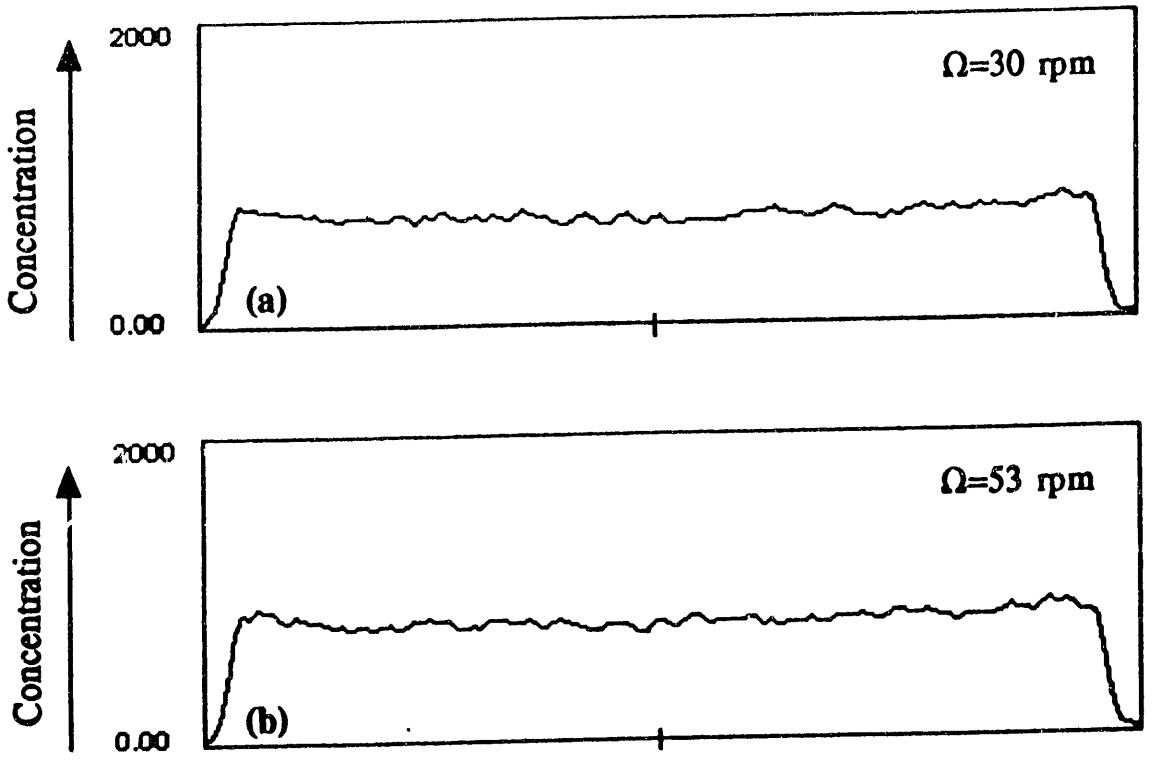
2000
Ω=30 rpm
Concentration
0.00
(a)
2000
Ω=53 rpm
Concentration
0.00
(b)

FIGURE 3

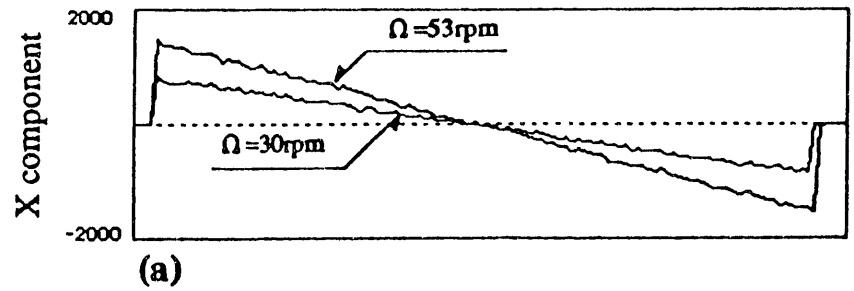
2000
-2000
X component
Ω=53rpm
Ω=30rpm

(a)

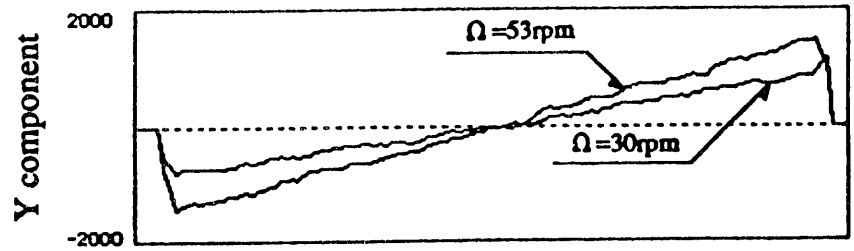
2000
-2000
Y component
Ω=53rpm
Ω=30rpm

(b)

FIGURE 4

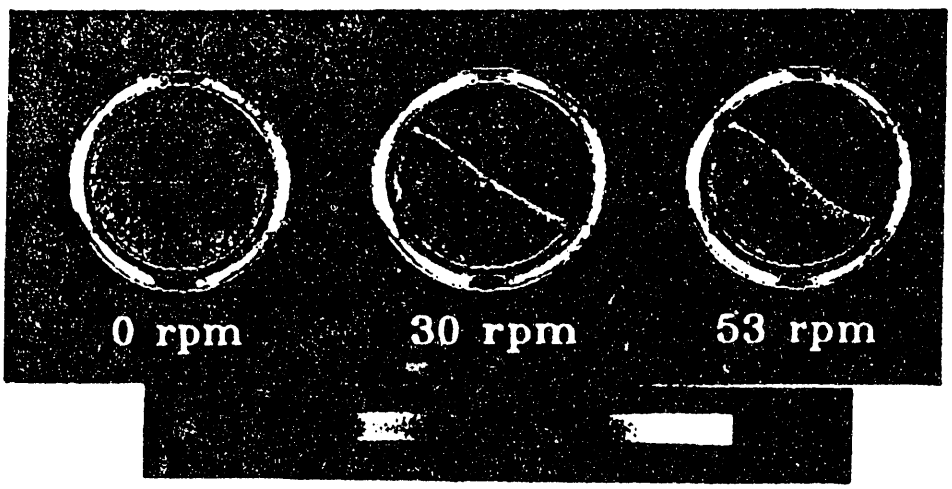

FIGURE 5

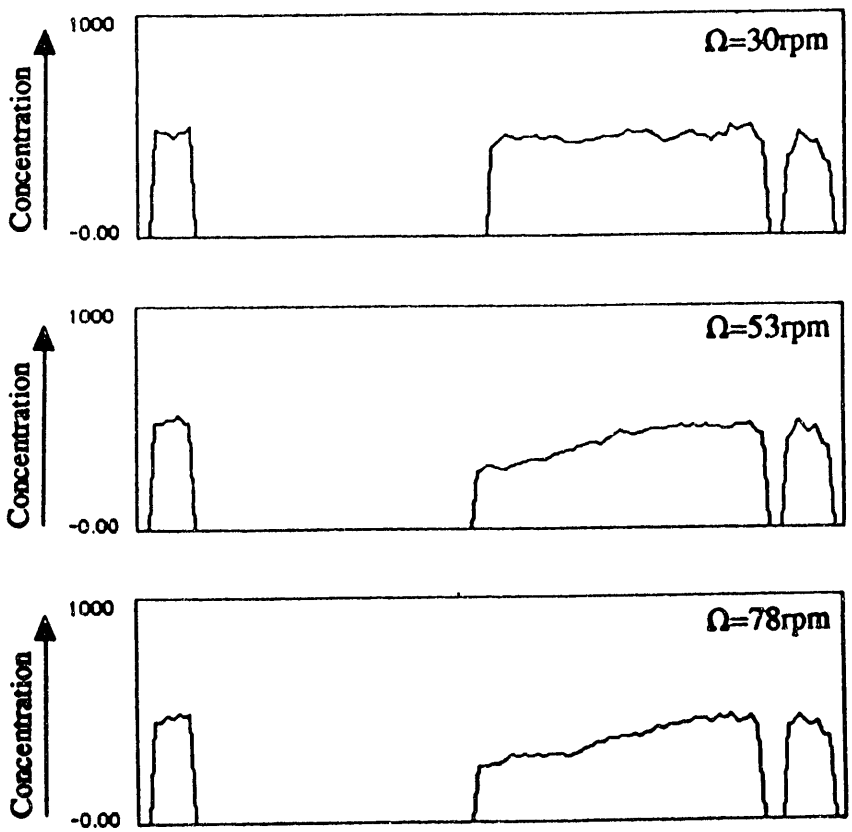
1000
Concentration
-0.00
Ω=30rpm
1000
Concentration
-0.00
Ω=53rpm
1000
Concentration
-0.00
Ω=78rpm

FIGURE 6

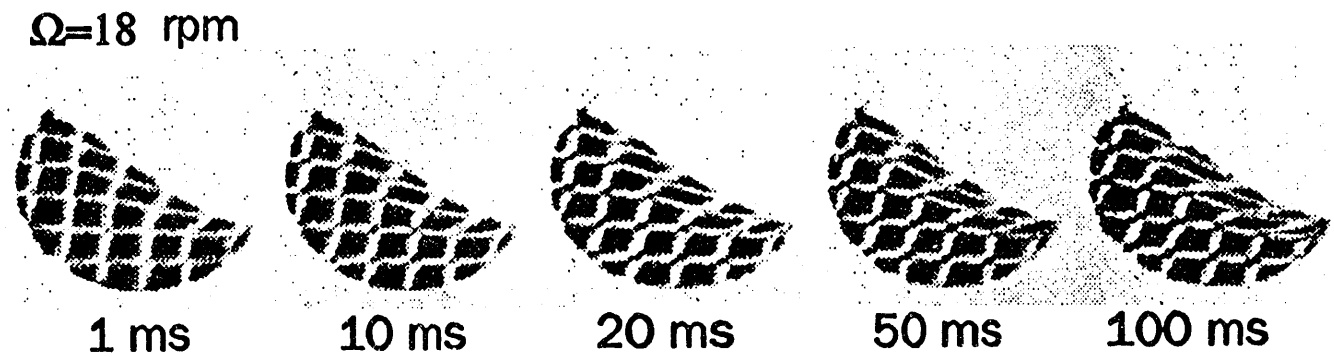

FIGURE 7

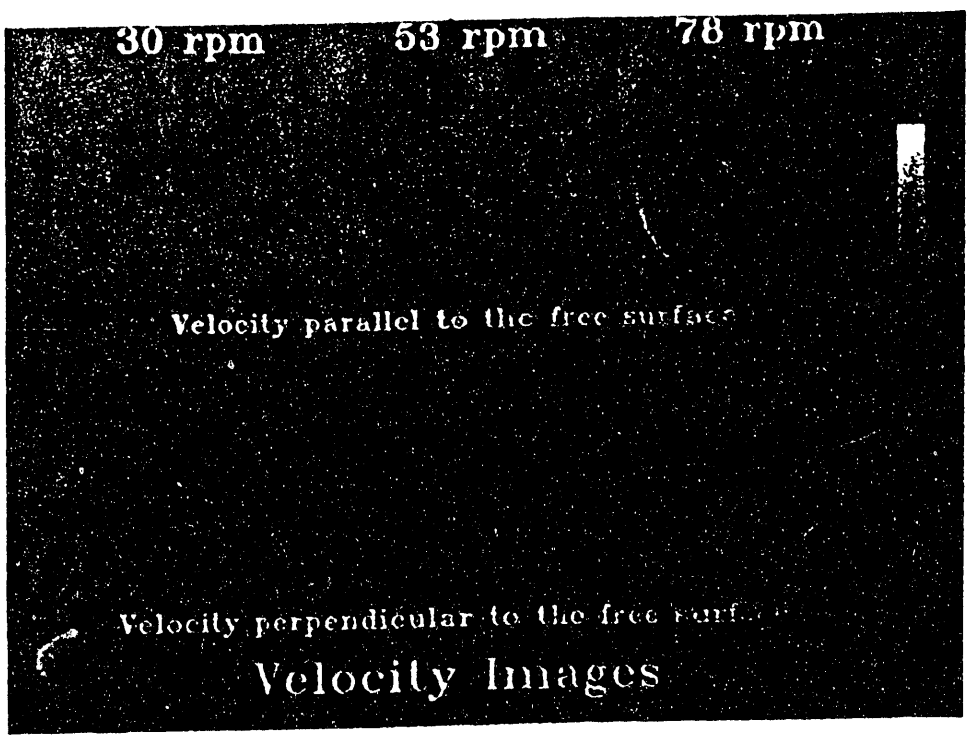
30 rpm
53 rpm
78 rpm
Velocity parallel to the free surface
Velocity perpendicular to the free surf
Velocity Images

FIGURE 8

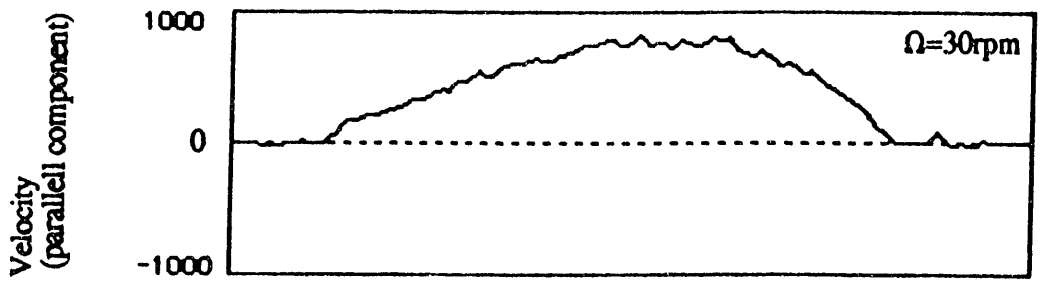

FIGURE 9

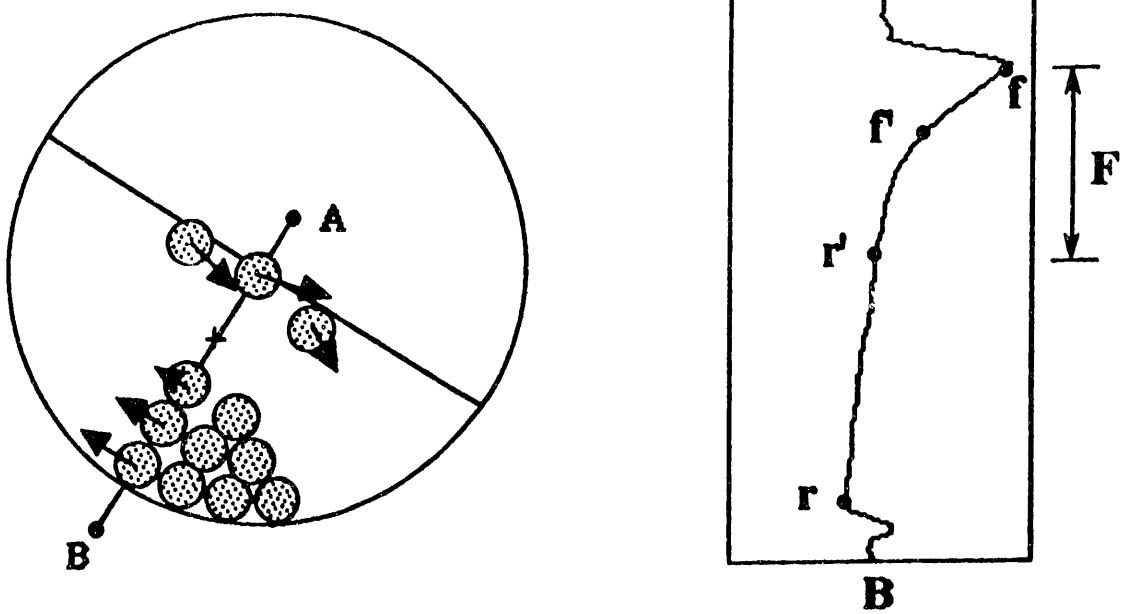

FIGURE 10

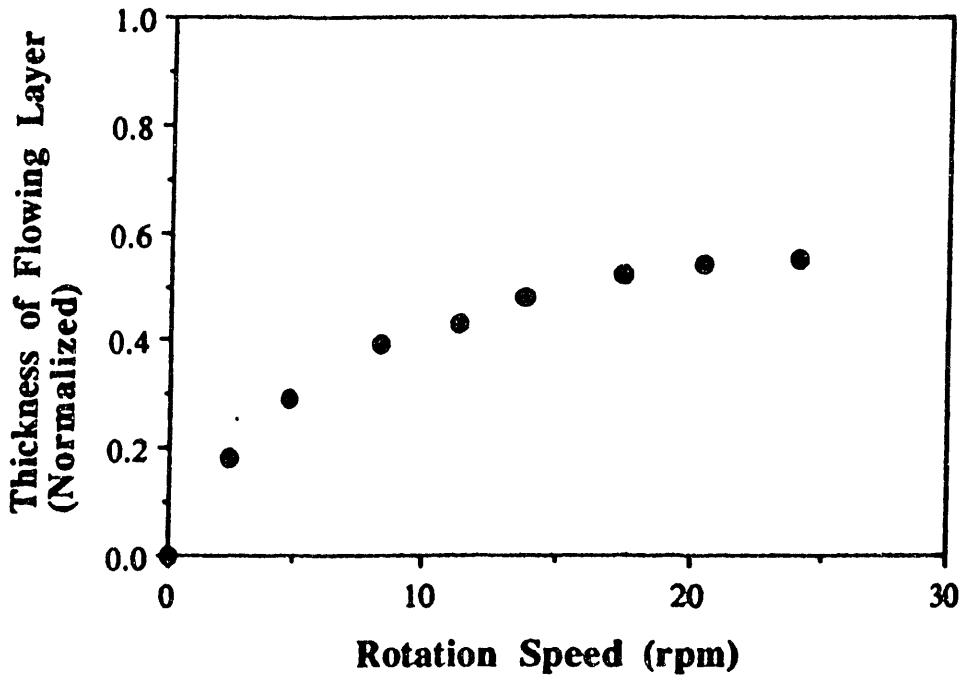
Thickness of Flowing Layer (Normalized)
1.0
0.8
0.6
0.4
0.2
0.0
0
10
20
30
Rotation Speed (rpm)

FIGURE 11

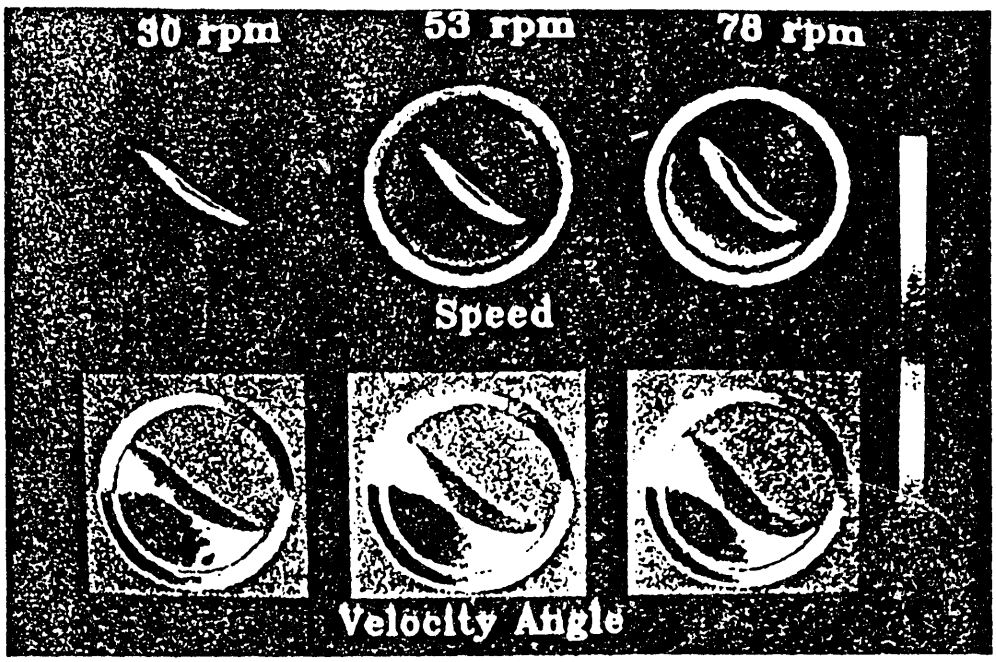

END

DATE
FILMED
5/04/93